Materials Science & Engineering B 236–237 (2018) 139–146

Contents lists available at ScienceDirect

Materials Science & Engineering B

journal homepage: www.elsevier.com/locate/mseb

Optical properties of ZnO deposited by atomic layer deposition (ALD) on Si nanowires

Octavio Graniel[a,1], Viktoriia Fedorenko[c,1], Roman Viter[c,d,*], Igor Iatsunskyi[e,*], Grzegorz Nowaczyk[e], Matthieu Weber[a], Karol Załęski[e], Stefan Jurga[e], Valentyn Smyntyna[b], Philippe Miele[a], Arunas Ramanavicius[d], Sebastien Balme[a], Mikhael Bechelany[a,*]

[a] Institut Européen des Membranes (IEM), UMR-5635, Université de Montpellier, ENSCM, CNRS, Place Eugène Bataillon, F-34095 Montpellier Cedex 5, France
[b] Faculty of Physics, Experimental Physics Department, Odessa National I.I. Mechnikov University, 42, Pastera 65026, Odessa, Ukraine
[c] Institute of Atomic Physics and Spectroscopy, University of Latvia, 19, Raina Blvd., LV 1586 Riga, Latvia
[d] Department of Physical Chemistry, Faculty of Chemistry and Geosciences, Vilnius University, Vilnius, Lithuania
[e] NanoBioMedical Centre, Adam Mickiewicz University, 85 Umultowska str., 61-614, Poznan, Poland

ARTICLE INFO

Keywords:
Silicon nanowires (SiNWs)
metal-assisted chemical etching (MACE)
nanosphere lithography (NSL)
atomic layer deposition (ALD)
ZnO

ABSTRACT

In this work, we report proof-of-concept results on the synthesis of Si core/ ZnO shell nanowires (SiNWs/ZnO) by combining nanosphere lithography (NSL), metal assisted chemical etching (MACE) and atomic layer deposition (ALD). The structural properties of the SiNWs/ZnO nanostructures prepared were investigated by X-ray diffraction, Raman spectroscopy, scanning and transmission electron microscopies. The X-ray diffraction analysis revealed that all samples have a hexagonal wurtzite structure. The grain sizes are found to be in the range of 7–14 nm. The optical properties of the samples were investigated using reflectance and photoluminescence spectroscopy. The study of photoluminescence (PL) spectra of SiNWs/ZnO samples showed the domination of defect emission bands, pointing to deviations of the stoichiometry of the prepared 3D ZnO nanostructures. Reduction of the PL intensity of the SiNWs/ZnO with the increase of SiNWs etching time was observed, depicting an advanced light scattering with the increase of the nanowire length. These results open up new prospects for the design of electronic and sensing devices.

1. Introduction

Silicon (Si) continues to be the most widely used semiconductor [1]. Such great interest in this material is due to its beneficial features such as high stability and non-toxicity, quantum confinement effects, high carrier mobility, and well-established fabrication technique [2]. Because of morphological and energetic features, silicon nanomaterials are one of the most studied types of nanomaterials. Nowadays, one dimensional (1D) silicon nanostructures, *i.e.*, silicon nanowires (SiNWs) and Si nanopillars, are of great interest because of their abilities to scatter and trap incident light, large surface to volume ratio, and other unique electronic and optical properties that make possible their use as promising blocks for a wide range of applications including electronic devices [3–5], energy storage devices [6,7], thermoelectrics [8–10], and biosensors [11–14].

The first preparation of Si whiskers with ⟨1 1 1⟩ orientation or filamentary Si crystals with macroscopic dimensions was reported in 1957 by Treuting and coworkers [15]. In 1964, Wagner and Ellis performed an illuminating work and established the vapor-liquid-solid (VLS) mechanism for the growth of Si whiskers [16]. These pioneering studies opened up exciting possibilities for the fabrication and investigation of SiNWs. In 2002, Peng and coworkers introduced an HF-etching-assisted nanoelectrochemical strategy to synthesize wafer-scale aligned SiNWs [17]. To date, there are many different techniques to produce SiNWs such as chemical vapor deposition using the VLS (Vapor—Liquid—Solid) mechanism [18], laser ablation [19], molecular beam epitaxy [20], chemical etching [21], and solution growth [22]. Among these preparation methods, the metal-assisted chemical etching (MACE) of silicon substrates in combination with nanosphere lithography (NSL) has recently emerged as a promising method to fabricate large areas of

* Corresponding authors at: Institute of Atomic Physics and Spectroscopy, University of Latvia, 19, Raina Blvd., LV 1586, Riga, Latvia (R. Viter). NanoBioMedical Centre, Adam Mickiewicz University, 85 Umultowska str., 61-614, Poznan, Poland (I. Iatsunskyi). Institut Européen des Membranes (IEM), UMR-5635, Université de Montpellier, ENSCM, CNRS, Place Eugène Bataillon, F-34095 Montpellier Cedex 5, France (M. Bechelany).
E-mail addresses: roman.viter@lu.lv (R. Viter), mikhael.bechelany@umontpellier.fr (M. Bechelany).
[1] Co-first authors.

https://doi.org/10.1016/j.mseb.2018.11.007
Received 6 October 2017; Received in revised form 11 October 2018; Accepted 21 November 2018
Available online 28 November 2018

ordered SiNWs [7,23]. The combination of MACE and NSL techniques is under increasing attention, mainly because MACE is an inexpensive and straightforward process that allows controlling various parameters of the etched nanostructures such as cross-sectional shape, diameter, length, and crystallographic orientation [24–26]. The main advantages of NSL are its short preparation time, high level of hexagonal structure orientation, and the possibility of application of large and monolayered masks directly onto different types of surfaces [27–29].

The addition of zinc oxide (ZnO) as shells around SiNWs (as cores) can have substantial and beneficial impact on the stability, as well as on the mechanical, photoelectrochemical, and sensing properties when compared to bare ZnO nanowires fabricated with other techniques [30–32]. Si wafer is an attractive substrate because of its low cost, good thermal conductivity, high crystalline quality, and availability of large size substrates with different types of conductivity (doping). Also, silicon is the best candidate for miniaturized electronic devices and the further development of modern nanoelectronic technology.

ZnO is a wide bandgap (3.4 eV) semiconductor, which has a stable wurtzite structure with lattice spacing $a = 0.325$ nm and $c = 0.521$ nm [33,34]. It has attracted intensive research effort for its unique properties such as thermal and chemical stability, optical transparency, and piezoelectricity [35].

ZnO thin films can be prepared using various techniques, but the conformality of the deposit required for its preparation as a shell around NWs requires the use of atomic layer deposition (ALD) [36–39]. ALD is a vapor phase deposition route based on self-limiting chemical reactions, allowing for the preparation of nanomaterials with controlled structures at the nanoscale [36,40–43]. The conformality, uniformity and atomic level control of the films that can be achieved using this technique makes it useful for a wide range of applications, especially microelectronics,[44] but also biosensing,[45] catalysis [46,47] and membranes.[48] Nowadays it is becoming a promising deposition method for growing uniform thin and ultra-thin films, especially in the cases where precise film thickness control, high reproducibility, thickness uniformity, and excellent conformity are required [45,49].

In the present work, silicon nanowires produced by gold-assisted chemical etching in combination with nanosphere lithography followed by an ALD deposition of ZnO are investigated. The structural and optical properties of the obtained nanostructures are evaluated.

2. Materials and methods

2.1. Materials

Microparticles based on polystyrene, size 1 μm, 10 wt% aqueous solution (89904), sodium dodecyl sulfate (436143), Hydrofluoric acid HF 40% (47590), Perdrogen H_2O_2 30% (31642), Nitric acid (30709), Hydrochloric acid (258148), Diethyl zinc (DEZ) ($Zn(CH_2CH_,)_2$, 95% purity, CAS: 557-20-0) were purchased from Sigma Aldrich. Boron-doped (8–25 Ω cm) p-type (1 0 0) crystal orientation Si wafers (LG Siltron Inc. Korea) were used as substrates.

2.2. Synthesis of SiNWs

The organized silicon nanowires were produced by gold-assisted chemical etching in combination with nanosphere lithography [23]. For this experiment, the monolayers were prepared with polystyrene particles (diameter 1 μm). The 1x1 and 2x2 cm^2 pieces of Si wafers were cleaned sequentially with deionized water (18.2 MΩ cm), ethanol and acetone by ultrasonication for 15 min in each solvent. Then the substrates were treated by O_2 plasma to have a hydrophilic surface. After the pretreatment, an ordered monolayer of polystyrene spheres (PSS) was prepared by self-assembly. The floating-transferring technique was utilized to deposit PSS on Si substrate. The polystyrene solution (40 μl) diluted by an equal amount of ethanol, was applied onto the modified substrate, which spread all over the substrate. After holding the substrate stationary for a while to obtain good dispersion of the suspension, the wafer was then slowly immersed into the glass vessel filled with deionized water and PSS started to form an unordered monolayer on the water surface. Then, one drop of 10% sodium dodecyl sulfate (SDS) solution was added to the water to change the surface tension and to consolidate the particles. The addition of SDS solution was an important step to produce 2D ordered colloidal array [50]. As a result, a large monolayer with highly ordered areas was obtained. Then this monolayer of PSS was transferred to the target substrate.

The quality of the PSS monolayer mask can be assessed right away by looking at the uniformity of the color throughout the whole area. The reflected color of the pattern varies with the size of the spheres and its quality. After the sample was dried in air at room temperature, the spheres were self-assembled into a close-packed, two-dimensional ordered lattice *via* attractive capillary forces [51,52]. Then the diameter of spheres was decreased by O_2 plasma etching for 5 min to expose the surface of the wafer for metal deposition. Plasma etching is capable of uniform and fast modification of nanospheres, and it can control the sphere diameter by adjusting the etching time [53]. In order to stick the PS spheres to the Si surface, a heat treatment at 100 °C for 30 min was performed. On the next step, a thin Au film was deposited by physical vapor deposition (PVD). The sputtering was carried out at a discharge of 25 mA in a vacuum with a pressure below 0.1 mbar. The samples covered by Au were etched with a solution of $H_2O/H_2O_2/HF$ with a volume ratio of 1:0.15:0.3 at room temperature for 1, 2, 5, and 7 min. To remove the metal, the samples were dipped in an aqua regia solution (a mixture of nitric acid and hydrochloric acid). After removing the Au, the PS spheres were etched by O_2 plasma. Fig. 1 represents the overall process for the synthesis of SiNWs.

2.3. ALD deposition of ZnO on Si NWs

A custom-made ALD reactor was used for the synthesis of ultrathin ZnO films. ALD was performed using sequential exposures of DEZ and H_2O separated by a purge of Argon with a flow rate of 100 standard cubic centimeters per minute (sccm). The deposition regime for ZnO consisted of 0.2 s pulse of DEZ, 40 s of exposure to DEZ, 60 s of purging

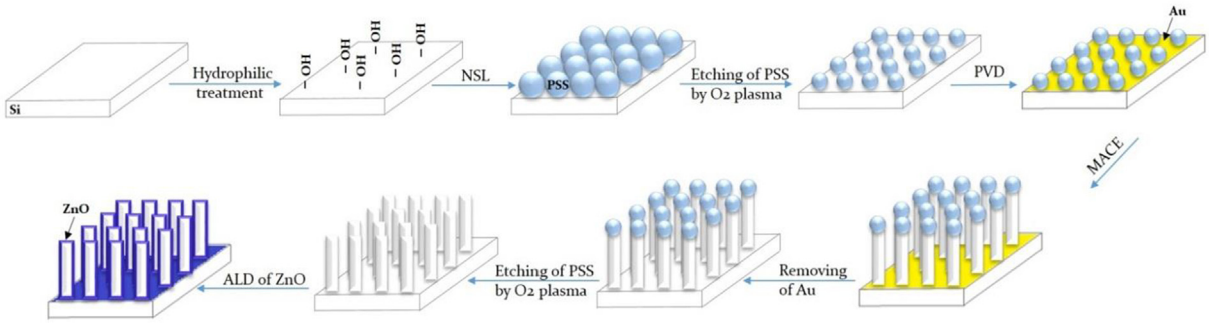

Fig. 1. Schematic representation of the fabrication of SiNWs by the combination of MACE and NSL.

with argon followed by 2 s pulse of H_2O, 40 s of exposure to H_2O, and finally 60 s of purging with argon. Thus, 20 and 50 nm thick ZnO layers were deposited on silicon nanowires using 100 and 250 ALD cycles, respectively. The deposition was performed at 100 °C. The typical growth rate for ZnO coating during these cycles was found to be 0.2 nm per cycle.

2.4. Characterization

Structural and chemical compositions of the SiNWs/ZnO were analyzed by scanning electron microscopy (SEM, S-4800, Hitachi), atomic force microscopy (AFM, NANOMAN 5 from Veeco controlled with the Nanoscope V software), and X-Ray diffraction (XRD, PANAlyticalXpert-PRO diffractometer equipped with a X'celerator detector using Ni-filteredCu Kα radiation). The XRD spectra were measured in the 2θ angular region between 10° and 60° with a scan speed of 2° min^{-1} and a step rate of roughly 0.02° per second. From the XRD spectra, the grain size was calculated using the Debye-Scherer equation. SiNWs covered by ALD of ZnO were also investigated by transmission electron microscopy (TEM) (JEOL ARM 200F high-resolution transmission electron microscope (200 kV) with an EDX analyzer). The cross-sections and lamellas for TEM investigations were prepared by Focused Ion Beam (FIB) with procedures described elsewhere [54]. The FIB milling was carried out with a JEOL, JIB-4000.

Raman scattering measurements were performed using a Renishaw micro-Raman spectrometer equipped with a confocal microscope (Leica). The samples were measured in backscattering geometry with a spectral resolution of 1.0 cm^{-1}. The incident light was not polarized, and also the light detector contained no polarization filters. The Raman scattering spectra were excited by a 488 nm laser. The beam was focused on the samples with a 50 × microscope objective with a numerical aperture of 0.4. The incident optical power was changed by using neutral density filters in the beam path.

Optical properties of the samples have been studied by diffuse reflectance spectroscopy (the spectral range 200–1400 nm). The diffuse reflectance spectroscopy has been performed using standard Shimadzu UV-3600 spectrophotometer with a scanning step of 1 nm. Photoluminescence spectroscopy was studied in the spectral range of 350–800 nm. The measurements were performed with a standard fluorometer (FS5 Spectrofluorometer (Edinburg instruments Ltd, 2 Bain Square, Kirkton Campus, EH54 7DQ, UK)). The excitation of luminescence was performed at a wavelength of 280 nm.

3. Results and discussion

Fig. 2 represents a dependence of the diameter of PSS as the function of different etching times by O_2 plasma (insets: 1 [Fig. 2b], 5 [Fig. 2c], and 10 min [Fig. 2d]). The etching of PSS by O_2 plasma from 1 to 10 min allows decreasing the PSS diameter from 960 ± 10 nm to 610 ± 10 nm. Fig. 2a shows the SEM image of PS spheres deposited on a Si wafer, which confirms the possibility to obtain a relatively large area, close-packed, hexagonal polystyrene monolayer produced by the floating-transferring technique. Fig. 2f shows a photograph of a monolayer pattern of PSS prepared by the mentioned technique on a 2x2 cm^2 silicon wafer. The color of the substrate observed in this photograph is due to the diffraction of light.

Fig. 3 shows the final structure of Si NWs (etching time is 5 min) after depositing 50 nm ZnO film by ALD. The SEM images indicate a conformal coating of Si substrate by ALD.

Fig. 4 shows (a) 2D and (b) 3D images of the SiNWs covered with a 50 nm ZnO layer by ALD. The array of SiNWs exhibit hexagonal packing over a large area of 15x15 μm as previously shown by SEM. Due to the high aspect ratio of the SiNWs, the AFM probe cannot reach the bottom part of the sample and degrades quickly. For this reason, the total length of the SiNWs cannot be seen by AFM and would require the use of exotic FIB milled tips and carbon nanotube/fiber tips [55].

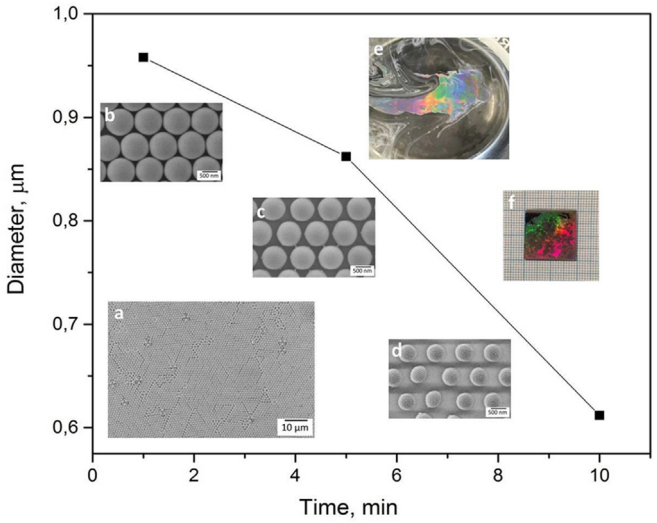

Fig. 2. Diameter of PSS as a function of the O_2 plasma etching time. The insets show SEM images of (a) a PSS monolayer prepared by the floating transferring technique, PSS after being etched by O_2 plasma for (b) 1 min, (c) 5 min, and (d) 10 min, and photographs of (e) a monolayer of PSS on the air-water interface and (f) on a 2x2 cm^2 silicon wafer.

XRD spectra of SiNWs (etched for 7 min) covered with 20 and 50 nm of ZnO by ALD are shown in Fig. 5. Three prominent peaks appear at 2θ = 31.78°, 34.35°, 36.25°, and 56.69°, which correspond to the (1 0 0), (0 0 2), (1 0 1), and (1 1 0) reflections of the hexagonal wurtzite phase of ZnO, respectively. This result indicates that both films are polycrystalline, as commonly reported for ZnO films deposited by ALD ([38,39,56]). A peak with low intensity at 2θ = 47.46° appears for the 50 nm thick sample, which corresponds to the (1 0 2) reflection of ZnO.

The grain sizes (D) of the deposited films are estimated using the following formula [34]:

$$D = \frac{0.9\lambda}{\beta\cos(\theta)}$$

where λ is the wavelength of X-ray used (λ = 0.154 nm), β is the full width at half maximum intensity in radians, and θ is the Bragg angle. The average value of grain size is found to be 7.5 ± 0.45 nm, and 14 ± 6.5 nm for samples etched for 7 min and covered with 20 and 50 nm of ZnO, respectively.

Fig. 6 shows the high-resolution TEM images of ZnO-Si nanowires with different ZnO layer thicknesses. Silicon nanowires coated with 20 nm of ZnO by ALD are presented in Fig. 5a. The TEM images show that the 20 nm ZnO layer covers conformally and homogenously the SiNWs. The distance between the nearest wires is narrowed to the bottom from 150 to 300 nm. We can notice that the diameter of the wires is about 450 nm on the top and 850 nm at the bottom. Thus, the wires have the shape of a truncated trapezoid. This shape could be due to the longer exposure time of the top part with the etching solution according to Dawood *et al.* [57]. Macroporous structure of the wires could also be observed (Fig. 6a). This can be explained by the lateral transport of the charge carriers [23].

Fig. 6b shows a TEM image of individual silicon nanowires covered by 50 nm ALD ZnO layer. The total thickness of the layer is approximately 50 nm (having amaximum value of 55 nm on the top). For both samples, the ZnO layers have a polycrystalline phase. The size of nanocrystallites was estimated using elliptical shape fitting, and the longer axis was used as the nanocrystallite size. The average grain size for the 50 and 20 nm ZnO layers was almost the same (11.8 ± 2.5 nm and 10 ± 2.5 nm, respectively). These results confirmed the data obtained by XRD. The TEM images demonstrate the ability to produce highly uniform layers of ZnO covered silicon nanowires by the ALD-

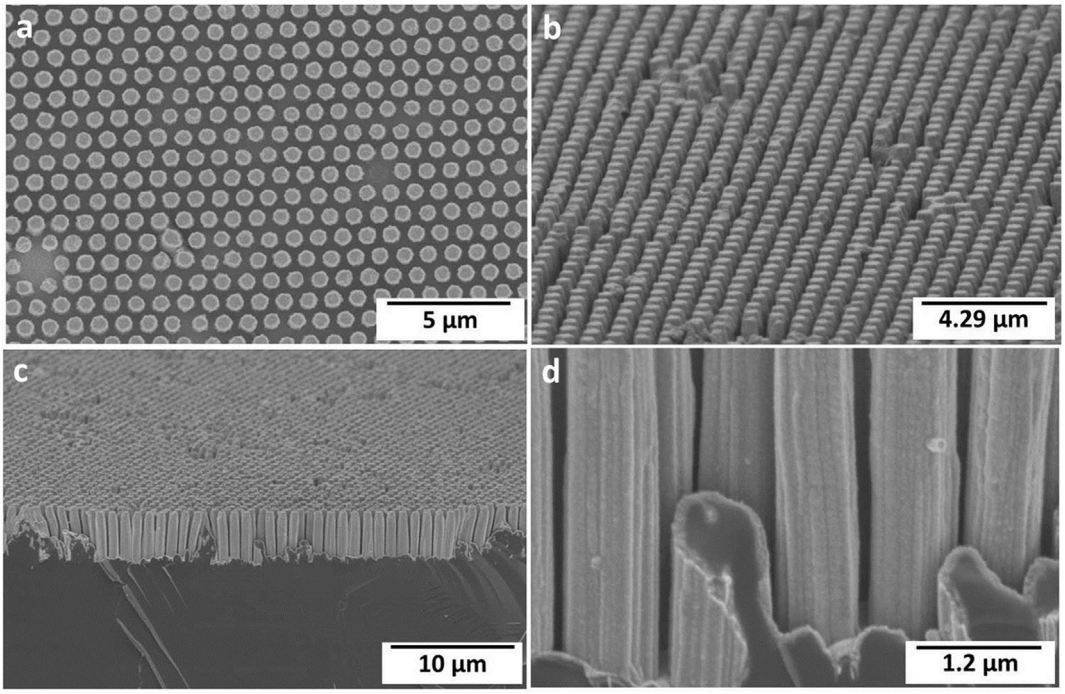

Fig. 3. SEM images of SiNWs (etched for 5 min) with a 50 nm ZnO layer deposited by ALD.

based process.

Raman spectroscopy was used to confirm the composition of SiNWs covered by ALD of ZnO. Fig. 7 shows the Raman spectra of Si nanowires (7 min. etching) with 20 and 50 nm of ZnO by ALD. An intense peak (E_2^{high} mode) of Si is observed at 520 cm^{-1} due to light penetrating through the thin ZnO films [58]. However, by increasing the number of accumulations, a Raman peak at 432 ± 2 cm^{-1} (E_2^{high} mode) that corresponds to the wurtzite phase of ZnO, was observed (inset of Fig. 7). This mode is associated with the motion of oxygen atoms [58-61]. The E_2^{high} mode peak (full width half maximum [FWHM] of ~ 20 cm^{-1}) is broader than the one for the bulk ZnO (FWHM is less than 10 cm^{-1}) and is shifted to higher frequencies or blue shifts. The broadening of the peak and the blue shift are attributed to phonon confinement effects [62].

Fig. 8 shows the reflectance of Si nanowires arrays etched for 2, 5 and 7 min and covered with (a) 20 and (b) 50 nm of ZnO, respectively. It was found that the reflectance decreases with the increase of the etching time,(which produces longer nanowires) as reported by others [63]. This decrease may be explained by the increased light trapping and absorption of longer nanowires [64]. We observed that the reflectance is less than 5% and 8% for the SiNWs (etched for 5 min) covered with ZnO 20 and 50 nm, respectively. This low reflectance could be explained by the energy band structure of the sample. The multiple band gaps in the system cause a variety of near band-edge absorptions from sunlight in different frequency ranges, reducing reflectivity. Also, the change of the refractive indexes of the materials may be related to the decrease of reflection[65,66]. . These excellent antireflective properties can be used to harvest photons in different applications such as solar cells [66], and laser-assisted desorption/ionization (LDI) measurements [67].

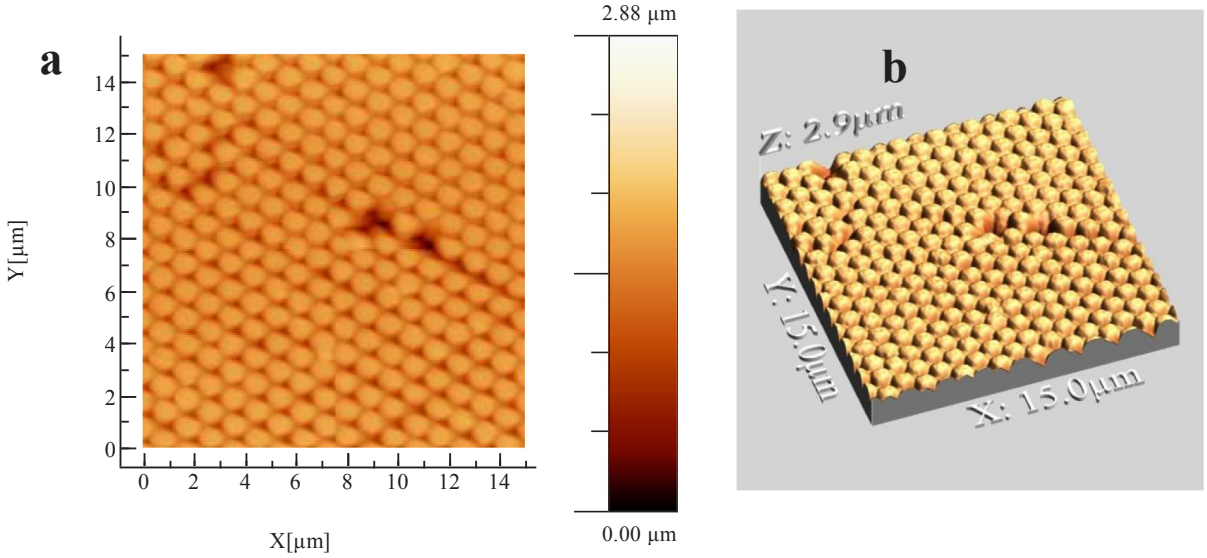

Fig. 4. (a) 2D and (b) 3D AFM images SiNWs covered with a 50 nm ZnO layer by ALD.

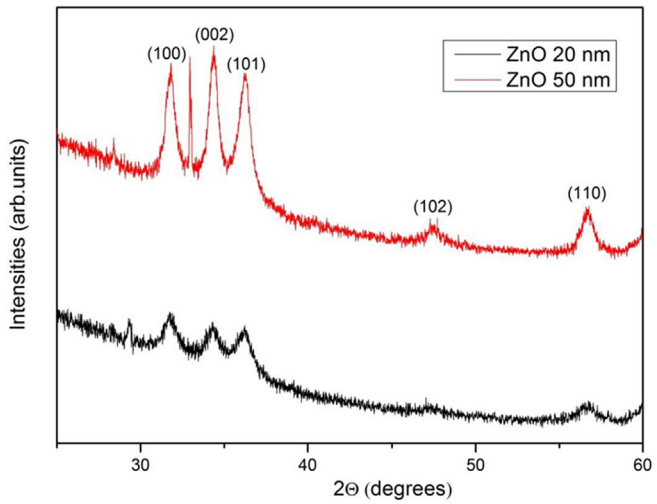

Fig. 5. XRD spectra of SiNWs/ZnO with different thicknesses (20 and 50 nm) of ZnO layers on SiNWs with 7 min etching. XRD spectra of SiNWs (etched for 7 min) covered with 20 and 50 nm of ZnO by ALD.

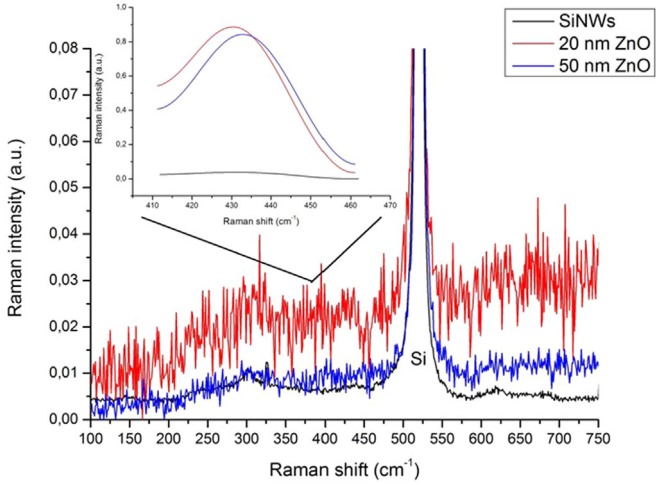

Fig. 7. Raman spectra of bare SiNWs (etched for 7 min) and after the deposition of ZnO (20 and 50 nm) by ALD.

The band gap values of SiNWs prepared at different etching times (2, 5 and 7 min) and covered with (a) 20 (and (b) 50 nm of ZnO by ALD, were graphically calculated in the linear part of the absorption edge and showed in Fig. 9. As we can see, the obtained values (presented in Table 1) are lower than the typical value of a ZnO single crystal (E_g = 3.37 eV). As reported before, this difference could be due to the concentration of point defects (such as vacancies and interstitials of Zn and O) [38]. We can also observe a small increase in the band gap value with the increase of the ZnO thickness. This could be associated with the improvement of the crystalline structure of the deposited samples [38].

The PL of 3D ZnO nanostructures with different thicknesses are plotted in Fig. 10. The PL spectra showed strong peaks in the range of 410–450 nm with a long PL tail going to higher wavelengths. Deconvolution of the PL spectra on separate lines has been performed using Gauss fitting in Origin software (see supporting information, Figure S1). The spectra deconvolution showed peaks centered at 376–379, 411–415, 434–437, 447–480, 490–540, 570–640 nm, and 660–740 nm related to free exciton, Zn interstitials, Zn vacancies, neutral oxygen vacancies, single charged oxygen vacancies, double charged oxygen vacancies, and surface defects, respectively [38,56,68,69]. The domination of defect emission bands points to deviations in the stoichiometry of the prepared 3D ZnO nanostructures. The decrease of PL intensity for ZnO samples deposited on 7 min etched SiNWs could be related to higher light scattering caused by their length. It is suggested that both the high surface area and the antireflective properties of the nanostructures might have an impact on the overall PL emission [64].

4. Conclusion

In summary, we have demonstrated a simple method for the fabrication of ordered aligned SiNWs/ZnO core shell nanostructures. The method utilizes a 2D non-close-packed polystyrene sphere template in combination with the MACE technique for the preparation of the NWs. Next, the conformal deposition of ZnO films as shells was performed on the highly-ordered vertical SiNWs array using the ALD route. The ordered SiNWs readily produced by the present method may find many applications in array devices such as field-effect transistors, sensors, electrodes, and two-dimensional photonic crystals. The high aspect ratio and anti-reflective characteristics inherent to the structure of the nanowires can be exploited for fabricating future nanoelectronic and optoelectronic devices. The detailed study of structural and optical properties of the core-shell SiNWs/ZnO heterostructures was presented. The X-ray diffraction analysis revealed that all samples have a

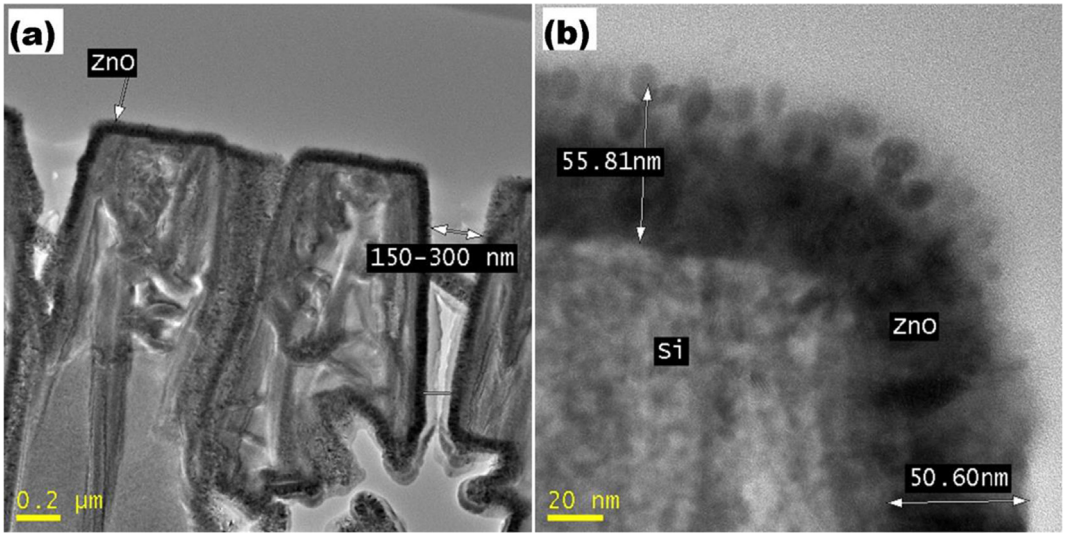

Fig. 6. Cross-sectional TEM images of SiNWswith (a) 20 and (b) 50 nm of ZnO by ALD.

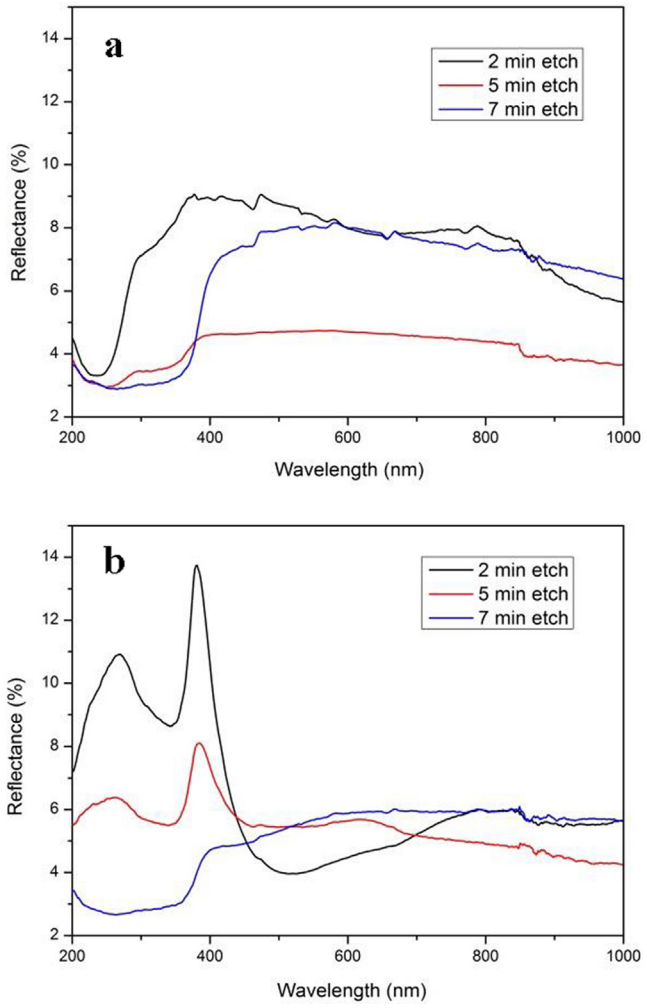

Fig. 8. Reflection spectra of SiNWs (etched for 2, 5, and 7 min) covered with (a) 20 and (b) 50 nm of ZnO by ALD.

hexagonal wurtzite structure. The grain sizes, as measured using XRD data, were found to be in the range of 7–14 nm and were confirmed by TEM. The TEM and SEM images demonstrated the ability to produce highly uniform layers of ZnO covered silicon nanowires by the ALD technique. The optical reflectance spectra for SiNWs/ZnO confirmed the low optical reflection of the thin films. The layer of ZnO on SiNWs can be applied as an antireflection coating. The study of photoluminescence (PL) spectra of SiNWs/ZnO showed the domination of defect emission bands, which points to deviations in thestoichiometry of the prepared 3D ZnO nanostructures. We also observed the reduction

Table 1
Band gap of SiNWs covered with 20 and 50 nm ZnO.

Etching time (min)	2	5	7
	E_g (eV)		
ZnO 20 nm	2.90 ± 5–7%	3.00 ± 5–7%	3.11 ± 5–7%
ZnO 50 nm	3.22 ± 5–7%	3.16 ± 5–7%	3.05 ± 5–7%

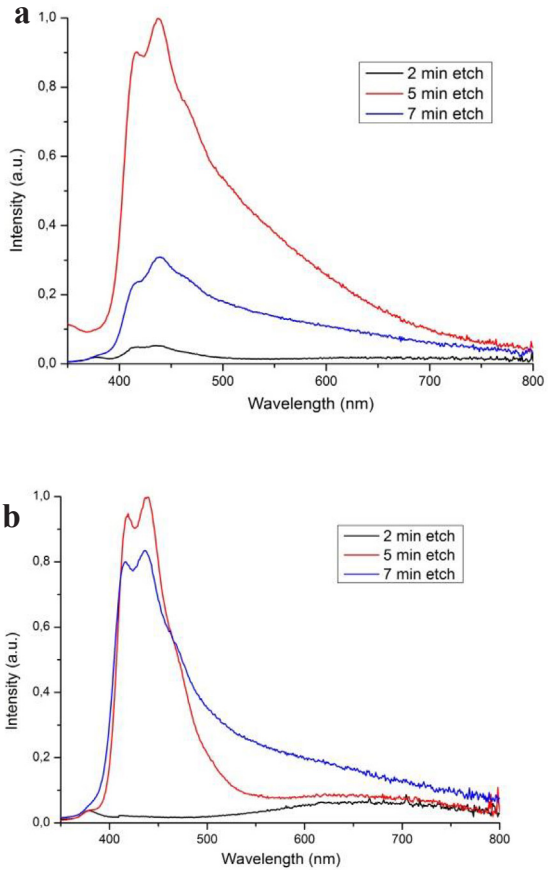

Fig. 10. Photoluminescence spectra of SiNWs (etched for 2, 5, and 7 min) covered with (a) 20 and (b) 50 nm of ZnO by ALD.

of the PL intensity of SiNWs/ZnO etched for 7 min that could be due to the higher light scattering caused by increasing the length of the nanowires. These results open new perspectives for the preparation of optical and sensing devices.

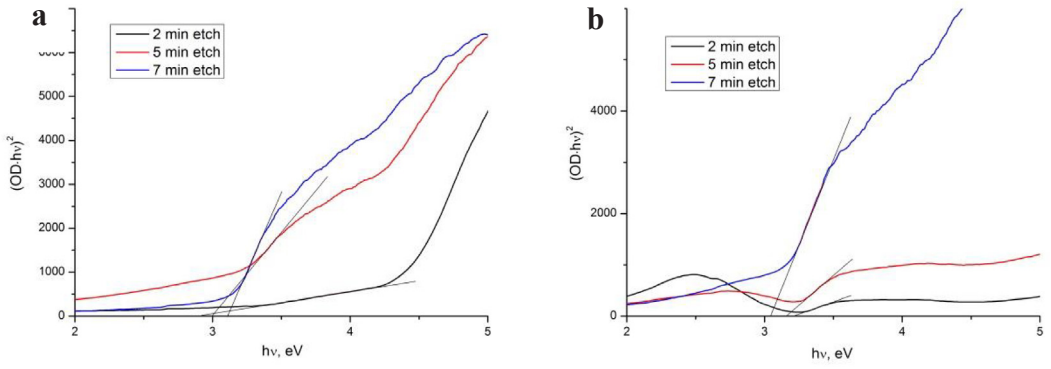

Fig. 9. Band gap estimation of SiNWs covered with (a) 20 nm and (b) 50 nm of ZnO layer by ALD.

Acknowledgments

R.V. acknowledges the financial support from the project '1D ZnO/Polidopamīna kodola čaulas nanostruktūru izstrāde ar uzlabotu jutību un uzlabotām struktūras, elektroniskajām un optiskajām īpašībām', within Latvian LZP fund (Reg. N. LZP 2018/1-0394) and the project 'Investigation of photoinduced processes in one dimentional ZnO/polydopamine nanostructures', within Latvian Post-doc program (Reg. N. ESS2018/295). I.I. acknowledges the financial support from the National Science Centre of Poland by the SONATA 11 project UMO-2016/21/D/ST3/00962. O.G. would like to thank CONACYT, México for funding. This work was supported by the European Union's Horizon 2020 research and innovation programme "CanBioSe" (grant agreement no. 778157).

Appendix A. Supplementary data

Supplementary data to this article can be found online at https://doi.org/10.1016/j.mseb.2018.11.007.

References

[1] Kim, K. 1.1 Silicon technologies and solutions for the data-driven world. In 2015 IEEE International Solid-State Circuits Conference - (ISSCC) Digest of Technical Papers; IEEE, 2015; Vol. 58, pp. 1–7.
[2] K.-Q. Peng, X. Wang, L. Li, Y. Hu, S.-T. Lee, Silicon nanowires for advanced energy conversion and storage, Nano Today 8 (2013) 75–97, https://doi.org/10.1016/j.nantod.2012.12.009.
[3] Y. Cui, Z. Zhong, D. Wang, W.U. Wang, C.M. Lieber, High Performance Silicon Nanowire Field Effect Transistors, Nano Lett. 3 (2003) 149–152, https://doi.org/10.1021/nl025875l.
[4] J. Goldberger, A.I. Hochbaum, R. Fan, P. Yang, Silicon Vertically Integrated Nanowire Field Effect Transistors, Nano Lett. 6 (2006) 973–977, https://doi.org/10.1021/nl060166j.
[5] L.J. Chen, Silicon nanowires: the key building block for future electronic devices, J. Mater. Chem. 17 (2007) 4639, https://doi.org/10.1039/b709983e.
[6] L.-F. Cui, R. Ruffo, C.K. Chan, H. Peng, Y. Cui, Crystalline-Amorphous Core − Shell Silicon Nanowires for High Capacity and High Current Battery Electrodes, Nano Lett. 9 (2009) 491–495, https://doi.org/10.1021/nl8036323.
[7] M. Pavlenko, E.L. Coy, M. Jancelewicz, K. Załęski, V. Smyntyna, S. Jurga, I. Iatsunskyi, Enhancement of optical and mechanical properties of Si nanopillars by ALD TiO_2 coating, RSC Adv. 6 (2016) 97070–97076, https://doi.org/10.1039/C6RA21742G.
[8] A.I. Hochbaum, R. Chen, R.D. Delgado, W. Liang, E.C. Garnett, M. Najarian, A. Majumdar, P. Yang, Enhanced thermoelectric performance of rough silicon nanowires, Nature 451 (2008) 163–167, https://doi.org/10.1038/nature06381.
[9] A.R. Abramson, W.C. Kim, S.T. Huxtable, H. Yan, Y. Wu, A. Majumdar, C.-L. Tien, P. Yang, Fabrication and Characterization of a Nanowire/Polymer-Based Nanocomposite for a Prototype Thermoelectric Device, J. Microelectromechanical Syst. 13 (2004) 505–513, https://doi.org/10.1109/JMEMS.2004.828742.
[10] A.I. Boukai, Y. Bunimovich, J. Tahir-Kheli, J.-K. Yu, W.A. Goddard III, J.R. Heath, Silicon nanowires as efficient thermoelectric materials, Nature 451 (2008) 168–171, https://doi.org/10.1038/nature06458.
[11] Y. Cui, Q. Wei, H. Park, C.M. Lieber, Nanowire nanosensors for highly sensitive and selective detection of biological and chemical species, Science 293 (2001) 1289–1292, https://doi.org/10.1126/science.1062711.
[12] D.R. Kim, X. Zheng, Numerical Characterization and Optimization of the Microfluidics for Nanowire Biosensors, Nano Lett. 8 (2008) 3233–3237, https://doi.org/10.1021/nl801559m.
[13] F. Patolsky, G. Zheng, C.M. Lieber, Nanowire-Based Biosensors, Anal. Chem. 78 (2006) 4260–4269, https://doi.org/10.1021/ac069419j.
[14] T.-E. Bae, H.-J. Jang, J.-H. Yang, W.-J. Cho, High Performance of Silicon Nanowire-Based Biosensors using a High- k Stacked Sensing Thin Film, ACS Appl. Mater. Interfaces 5 (2013) 5214–5218, https://doi.org/10.1021/am401026z.
[15] R.G. Treuting, S.M. Arnold, Orientation habits of metal whiskers, Acta Metall. 5 (1957) 598, https://doi.org/10.1016/0001-6160(57)90128-1.
[16] R.S. Wagner, W.C. Ellis, Vapor-liquid-solid mechanism of single crystal growth, Appl. Phys. Lett. 4 (1964) 89–90, https://doi.org/10.1063/1.1753975.
[17] K.-Q. Peng, Y.-J. Yan, S.-P. Gao, J. Zhu, Synthesis of Large-Area Silicon Nanowire Arrays via Self-Assembling Nanoelectrochemistry, Adv. Mater. 14 (2002) 1164, https://doi.org/10.1002/1521-4095(20020816)14:16<1164::AID-ADMA1164>3.0.CO;2-E.
[18] D. Lerose, M. Bechelany, L. Philippe, J. Michler, S. Christiansen, Ordered arrays of epitaxial silicon nanowires produced by nanosphere lithography and chemical vapor deposition, J. Cryst. Growth 312 (2010) 2887–2891, https://doi.org/10.1016/j.jcrysgro.2010.07.023.
[19] N. Fukata, T. Oshima, T. Tsurui, S. Ito, K. Murakami, Synthesis of silicon nanowires using laser ablation method and their manipulation by electron beam, Sci. Technol. Adv. Mater. 6 (2005) 628–632, https://doi.org/10.1016/j.stam.2005.06.015.
[20] B. Fuhrmann, H.S. Leipner, H.-R. Höche, L. Schubert, P. Werner, U. Gösele, Ordered Arrays of Silicon Nanowires Produced by Nanosphere Lithography and Molecular Beam Epitaxy, Nano Lett. 5 (2005) 2524–2527, https://doi.org/10.1021/nl051856a.
[21] Y.J. Zhang, W. Li, K.J. Chen, Application of two-dimensional polystyrene arrays in the fabrication of ordered silicon pillars, J. Alloys Compd. 450 (2008) 512–516, https://doi.org/10.1016/j.jallcom.2006.11.184.
[22] N.-M. Park, C.-J. Choi, Growth of silicon nanowires in aqueous solution under atmospheric pressure, Nano Res. 7 (2014) 898–902, https://doi.org/10.1007/s12274-014-0451-x.
[23] M. Bechelany, E. Berodier, X. Maeder, S. Schmitt, J. Michelr, L. Philippe, New silicon architectures by gold-assisted chemical etching, ACS Appl. Mater. Interfaces 3 (2011) 3866–3873, https://doi.org/10.1021/am200948p.
[24] Z. Huang, N. Geyer, P. Werner, J. de Boor, U. Gösele, Metal-Assisted Chemical Etching of Silicon: A Review, Adv. Mater. 23 (2011) 285–308, https://doi.org/10.1002/adma.201001784.
[25] H. Han, Z. Huang, W. Lee, Metal-assisted chemical etching of silicon and nanotechnology applications, Nano Today 9 (2014) 271–304, https://doi.org/10.1016/j.nantod.2014.04.013.
[26] N. Geyer, N. Wollschläger, B. Fuhrmann, A. Tonkikh, A. Berger, P. Werner, M. Jungmann, R. Krause-Rehberg, H.S. Leipner, Influence of the doping level on the porosity of silicon nanowires prepared by metal-assisted chemical etching, Nanotechnology 26 (2015) 245301, , https://doi.org/10.1088/0957-4484/26/24/245301.
[27] J. Rybczynski, M. Hilgendorff, Giersig M. Nanosphere, Lithography — Fabrication of Various Periodic Magnetic Particle Arrays Using Versatile Nanosphere Masks, Low-Dimensional Systems: Theory, Preparation, and Some Applications, Springer, Netherlands: Dordrecht, 2003, pp. 163–172.
[28] P. Colson, C. Henrist, R. Cloots, Nanosphere Lithography: A Powerful Method for the Controlled Manufacturing of Nanomaterials, J. Nanomater. 2013 (2013) 1–19, https://doi.org/10.1155/2013/948510.
[29] E.M. Akinoglu, A.J. Morfa, M. Giersig, Nanosphere lithography - Exploiting self-assembly on the nanoscale for sophisticated nanostructure fabrication, Turkish J. Phys. 38 (2014) 563–572, https://doi.org/10.3906/fiz-1407-9.
[30] H.-H. Li, C.-E. Yang, C.-C. Kei, C.-Y. Su, W.-S. Dai, J.-K. Tseng, P.-Y. Yang, J.-C. Chou, H.-C. Cheng, Coaxial-structured ZnO/silicon nanowires extended-gate field-effect transistor as pH sensor, Thin Solid Films 529 (2013) 173–176, https://doi.org/10.1016/j.tsf.2012.05.045.
[31] E. Memarzadeh Lotfabad, P. Kalisvaart, K. Cui, A. Kohandehghan, M. Kupsta, B. Olsen, D. Mitlin, ALD TiO2 coated silicon nanowires for lithium ion battery anodes with enhanced cycling stability and coulombic efficiency, Phys. Chem. Chem. Phys. 15 (2013) 13646, https://doi.org/10.1039/c3cp52485j.
[32] Z. Chen, G. Ma, Z. Chen, Y. Zhang, Z. Zhang, J. Gao, Q. Meng, M. Yuan, X. Wang, J. Liu, G. Zhou, Fabrication and photoelectrochemical properties of silicon nanowires/g-C3N4 core/shell arrays, Appl. Surf. Sci. 396 (2017) 609–615, https://doi.org/10.1016/J.APSUSC.2016.10.203.
[33] M. Bechelany, A. Amin, A. Brioude, D. Cornu, P. Miele, ZnO nanotubes by template-assisted sol-gel route, J. Nanoparticle Res. 14 (2012) 980, https://doi.org/10.1007/s11051-012-0980-8.
[34] E. Robak, E. Coy, M. Kotkowiak, S. Jurga, K. Załęski, H. Drozdowski, The effect of Cu doping on the mechanical and optical properties of zinc oxide nanowires synthesized by hydrothermal route, Nanotechnology 27 (2016) 175706, , https://doi.org/10.1088/0957-4484/27/17/175706.
[35] Ü. Özgür, Y.I. Alivov, C. Liu, A. Teke, M.A. Reshchikov, S. Doğan, V. Avrutin, S.-J. Cho, H. Morkoç, A comprehensive review of ZnO materials and devices, J. Appl. Phys. 98 (2005) 41301, https://doi.org/10.1063/1.1992666.
[36] M. Steven, George Atomic Layer Deposition: An Overview, Chem. Rev. 110 (2010) 111–131, https://doi.org/10.1021/cr900056b.
[37] M. Leskelä, M. Ritala, Atomic layer deposition (ALD): From precursors to thin film structures. In *Thin Solid Films*, Elsevier 409 (2002) 138–146.
[38] A.A. Chaaya, R. Viter, M. Bechelany, Z. Alute, D. Erts, A. Zalesskaya, K. Kovalevskis, V. Rouessac, V. Smyntyna, P. Miele, Evolution of microstructure and related optical properties of ZnO grown by atomic layer deposition, Beilstein J. Nanotechnol. 4 (2013) 690–698, https://doi.org/10.3762/bjnano.4.78.
[39] R. Viter, A.A. Chaaya, I. Iatsunskyi, G. Nowaczyk, K. Kovalevskis, D. Erts, P. Miele, V. Smyntyna, M. Bechelany, Tuning of ZnO 1D nanostructures by atomic layer deposition and electrospinning for optical gas sensor applications, Nanotechnology 26 (2015) 105501, , https://doi.org/10.1088/0957-4484/26/10/105501.
[40] C. Marichy, M. Bechelany, N. Pinna, Atomic layer deposition of nanostructured materials for energy and environmental applications, Adv. Mater. 24 (2012) 1017–1032, https://doi.org/10.1002/adma.201104129.
[41] M.J. Weber, A.J.M. Mackus, M.A. Verheijen, C. van der Marel, W.M.M. Kessels, Supported Core/Shell Bimetallic Nanoparticles Synthesis by Atomic Layer Deposition, Chem. Mater. 24 (2012) 2973–2977, https://doi.org/10.1021/cm301206e.
[42] M. Weber, I. Iatsunskyi, E. Coy, P. Miele, D. Cornu, M. Bechelany, Novel and Facile Route for the Synthesis of Tunable Boron Nitride Nanotubes Combining Atomic Layer Deposition and Annealing Processes for Water Purification, Adv. Mater. Interfaces 5 (2018) 1800056, https://doi.org/10.1002/admi.201800056.
[43] M.J. Weber, M.A. Verheijen, A.A. Bol, W.M.M. Kessels, Sub-nanometer dimensions control of core/shell nanoparticles prepared by atomic layer deposition, Nanotechnology 26 (2015) 94002, https://doi.org/10.1088/0957-4484/26/9/094002.
[44] I.J. Raaijmakers, Current and Future Applications of ALD in Micro-electronics, ECS Trans. 41 (2011) 3–17, https://doi.org/10.1149/1.3633649.
[45] O. Graniel, M. Weber, S. Balme, P. Miele, M. Bechelany, Atomic layer deposition for

biosensing applications, Biosens. Bioelectron. 122 (2018) 147–159, https://doi.org/10.1016/j.bios.2018.09.038.
[46] M. Weber, P. Collot, H. El Gaddari, S. Tingry, M. Bechelany, Y. Holade, Enhanced Catalytic Glycerol Oxidation Activity Enabled by Activated-Carbon-Supported Palladium Catalysts Prepared through Atomic Layer Deposition, ChemElectroChem 5 (2018) 743–747, https://doi.org/10.1002/celc.201701196.
[47] A.J.M. Mackus, M.J. Weber, N.F.W. Thissen, D. Garcia-Alonso, R.H.J. Vervuurt, S. Assali, A.A. Bol, M.A. Verheijen, W.M.M. Kessels, Atomic layer deposition of Pd and Pt nanoparticles for catalysis: on the mechanisms of nanoparticle formation, Nanotechnology 27 (2016) 34001, https://doi.org/10.1088/0957-4484/27/3/034001.
[48] M. Weber, A. Julbe, A. Ayral, P. Miele, M. Bechelany, Atomic layer deposition for membranes: Basics, challenges, and opportunities, Chem. Mater. 30 (2018) 7368–7390, https://doi.org/10.1021/acs.chemmater.8b02687.
[49] I. Iatsunskyi, M. Jancelewicz, G. Nowaczyk, M. Kempiński, B. Peplińska, M. Jarek, K. Załęski, S. Jurga, V. Smyntyna, Atomic layer deposition TiO_2 coated porous silicon surface: Structural characterization and morphological features, Thin Solid Films 589 (2015) 303–308, https://doi.org/10.1016/j.tsf.2015.05.056.
[50] Y. Zhang, X. Wang, Y. Wang, H. Liu, J. Yang, Ordered nanostructures array fabricated by nanosphere lithography, J. Alloys Compd. 452 (2008) 473–477, https://doi.org/10.1016/j.jallcom.2007.11.021.
[51] P.A. Kralchevsky, K. Nagayama, Capillary forces between colloidal particles, Langmuir 10 (1994) 23–36, https://doi.org/10.1021/la00013a004.
[52] K.D. Danov, B. Pouligny, P.A. Kralchevsky, Capillary Forces between Colloidal Particles Confined in a Liquid Film: The Finite-Meniscus Problem, Langmuir 17 (2001) 6599–6609, https://doi.org/10.1021/la0107300.
[53] S.S. Shinde, S. Park, Oriented colloidal-crystal thin films of polystyrene spheres via spin coating, J. Semicond. 36 (2015) 23001, https://doi.org/10.1088/1674-4926/36/2/023001.
[54] I. Iatsunskyi, E. Coy, R. Viter, G. Nowaczyk, M. Jancelewicz, I. Baleviciute, K. Załęski, S. Jurga, Study on Structural, Mechanical, and Optical Properties of Al_2O_3 –TiO_2 Nanolaminates Prepared by Atomic Layer Deposition, J. Phys. Chem. C 119 (2015) 20591–20599, https://doi.org/10.1021/acs.jpcc.5b06745.
[55] B.A. Bryce, B. Robert Ilic, M.C. Reuter, S. Tiwari, Silicon nanowire atomic force microscopy probes for high aspect ratio geometries, Appl. Phys. Lett. 100 (2012) 213106, , https://doi.org/10.1063/1.4720406.
[56] A.A. Chaaya, R. Viter, I. Baleviciute, M. Bechelany, A. Ramanavicius, Z. Gertnere, D. Erts, V. Smyntyna, P. Miele, Tuning Optical Properties of Al_2O_3/ZnO Nanolaminates Synthesized by Atomic Layer Deposition, J. Phys. Chem. C 118 (2014) 3811–3819, https://doi.org/10.1021/jp411970w.
[57] M.K. Dawood, T.H. Liew, P. Lianto, M.H. Hong, S. Tripathy, J.T.L. Thong, W.K. Choi, Interference lithographically defined and catalytically etched, large-area silicon nanocones from nanowires, Nanotechnology 21 (2010) 205305, , https://doi.org/10.1088/0957-4484/21/20/205305.
[58] J. Ye, S. Gu, S. Zhu, T. Chen, W. Liu, F. Qin, L. Hu, R. Zhang, Y. Shi, Y. Zheng, Raman and photoluminescence of ZnO films deposited on Si (111) using low-pressure metalorganic chemical vapor deposition, J. Vac. Sci. Technol. A Vacuum, Surfaces, Film 21 (2003) 979–982, https://doi.org/10.1116/1.1580836.
[59] B. Pal, P.K. Giri, Defect Mediated Magnetic Interaction and High T_c Ferromagnetism in Co Doped ZnO Nanoparticles, J. Nanosci. Nanotechnol. 11 (2011) 9167–9174, https://doi.org/10.1166/jnn.2011.4293.
[60] G. Mohan Kumar, P. Ilanchezhiyan, J. Kawakita, M. Subramanian, R. Jayavel, Magnetic and optical property studies on controlled low-temperature fabricated one-dimensional Cr doped ZnO nanorods, CrystEngComm 2010 (1887) 12, https://doi.org/10.1039/b924643f.
[61] S. Kuriakose, B. Satpati, S. Mohapatra, Enhanced photocatalytic activity of Co doped ZnO nanodisks and nanorods prepared by a facile wet chemical method, Phys. Chem. Chem. Phys. 16 (2014) 12741, https://doi.org/10.1039/c4cp01315h.
[62] I. Iatsunskyi, M. Pavlenko, R. Viter, M. Jancelewicz, G. Nowaczyk, I. Baleviciute, K. Załęski, S. Jurga, A. Ramanavicius, V. Smyntyna, Tailoring the Structural, Optical, and Photoluminescence Properties of Porous Silicon/TiO 2 Nanostructures, J. Phys. Chem. C 119 (2015) 7164–7171, https://doi.org/10.1021/acs.jpcc.5b01670.
[63] Y. Cao, A. Liu, H. Li, Y. Liu, F. Qiao, Z. Hu, Y. Sang, Fabrication of silicon wafer with ultra low reflectance by chemical etching method, Appl. Surf. Sci. 257 (2011) 7411–7414, https://doi.org/10.1016/J.APSUSC.2011.02.102.
[64] Y.-M. Chang, S.-R. Jian, H.-Y. Lee, C.-M. Lin, J.-Y. Juang, Enhanced visible photoluminescence from ultrathin ZnO films grown on Si-nanowires by atomic layer deposition, Nanotechnology 21 (2010) 385705, , https://doi.org/10.1088/0957-4484/21/38/385705.
[65] Q. Yang, D. Li, B. Yu, S. Huang, J. Wang, S. Li, J. Kang, Size effect on morphology and optical properties of branched ZnO/Si nanowire arrays, Phys. Lett. A 380 (2016) 1044–1048, https://doi.org/10.1016/j.physleta.2016.01.006.
[66] J.-Y. Jung, Z. Guo, S.-W. Jee, H.-D. Um, K.-T. Park, J.-H. Lee, A strong antireflective solar cell prepared by tapering silicon nanowires, Opt. Express 18 (2010) A286, https://doi.org/10.1364/OE.18.00A286.
[67] I. Kurylo, A. Hamdi, A. Addad, R. Boukherroub, Y. Coffinier, I. Kurylo, A. Hamdi, A. Addad, R. Boukherroub, Y. Coffinier, Comparison of Ti-Based Coatings on Silicon Nanowires for Phosphopeptide Enrichment and Their Laser Assisted Desorption/Ionization Mass Spectrometry Detection, Nanomaterials 7 (2017) 272, https://doi.org/10.3390/nano7090272.
[68] R. Viter, Z. Balevicius, A. Abou Chaaya, I. Baleviciute, S. Tumenas, L. Mikoliunaite, A. Ramanavicius, Z. Gertnere, A. Zalesska, V. Vataman, V. Smyntyna, D. Erts, P. Miele, M. Bechelany, The influence of localized plasmons on the optical properties of Au/ZnO nanostructures, J. Mater. Chem. C 3 (2015) 6815–6821, https://doi.org/10.1039/C5TC00964B.
[69] R. Viter, I. Iatsunskyi, V. Fedorenko, S. Tumenas, Z. Balevicius, A. Ramanavicius, S. Balme, M. Kempiński, G. Nowaczyk, S. Jurga, M. Bechelany, Enhancement of Electronic and Optical Properties of ZnO/Al_2O_3 Nanolaminate Coated Electrospun Nanofibers, J. Phys. Chem. C 120 (2016) 5124–5132, https://doi.org/10.1021/acs.jpcc.5b12263.